Journal of Power Sources 206 (2012) 402–408

Contents lists available at SciVerse ScienceDirect

Journal of Power Sources

journal homepage: www.elsevier.com/locate/jpowsour

High temperature versus low temperature Zebra ($Na/NiCl_2$) cell performance

Mehdi Hosseinifar, Anthony Petric*

Department of Materials Science and Engineering, McMaster University, 1280 Main St. W., Hamilton, Ontario L8S 4L7, Canada

ARTICLE INFO

Article history:
Received 8 November 2011
Received in revised form 20 January 2012
Accepted 21 January 2012
Available online 28 January 2012

Keywords:
Sodium/nickel chloride battery
Cycle life assessment

ABSTRACT

The effect of operating temperature on performance and aging of Zebra cells was investigated. The cells were cycled at 260 °C and 350 °C using a modified charging regime to accelerate damage. The cathode and solid electrolyte of degraded cells at the end of cycling were analyzed by scanning electron microscopy, energy dispersive spectroscopy and X-ray diffraction. It is hypothesized that the formation of AlF_3 on the surface of the β″ alumina electrolyte contributes to the failure of cells at low temperatures. A mechanism based on the overcharge reaction is proposed for the formation of this phase. At 350 °C, a significant capacity loss was observed with cycle life, which correlates to nickel particle growth as the cause of this phenomenon. The factors responsible for Ni grain growth are discussed.

1. Introduction

The Zebra ($Na/NiCl_2$) battery with high energy density, high durability and zero electrochemical self-discharge is a candidate for electric vehicle traction and grid energy storage. The increased demand for green energy sources such as wind turbines and photovoltaics which are inherently intermittent has intensified the need for batteries with high specific energy characteristics. Improving energy density of the Zebra battery was recently proposed through a new cell design [1,2]. However to date, these cells are commercially produced solely by Fiamm SoNick, Stabio, Switzerland. General Electric has announced plans to start production of Zebra cells in the near future which makes use of the standard design. While the design and chemistry of the cells fabricated by Fiamm SoNick are well known [3–8], there are few data available in the literature on the aging process and failure mechanism of these cells.

Lifespan of a rechargeable battery depends on the cycling conditions such as temperature, charging regime, depth of discharge (DoD), discharge rate, and so on. In order to prolong the cycle life of these cells, an IU charging regime is recommended by Fiamm SoNick. In this regime, charging starts with constant 10 A current until the cell voltage reaches 2.67 V. Then, the voltage is maintained at 2.67 V with the current gradually dropping. The cell is considered fully charged when the current drops below 0.5 A [7]. Zebra cells have been shown to undergo thousands of cycles with this regime [9]. The Zebra cell operates in the range of 260–350 °C. The lower temperature limit is dictated by the kinetics of solid state reactions in the cathode and by the sodium ion conductivity of the β″ solid electrolyte. The conductivity of β″ alumina reaches a reasonable value of 0.2 S cm^{-1} at 260 °C [8]. The upper temperature limit is set to avoid excessive dissolution of the $FeCl_2$ in the $NaAlCl_4$ molten electrolyte. This could result in the degradation of the solid electrolyte and hence increase in the resistance of the cell in case the dissolved Fe ions exchange with Na ions of the β″-alumina [10]. In practice, the Zebra batteries run at 275 °C with transient excursions up to 330 °C during high current discharge due to self-heating of the battery pack.

In the present work, the simultaneous effect of temperature and high charging voltage on the performance and failure of Zebra cells was investigated. Zebra cells were cycled at the extremes of temperature range and their behavior is explained based on microstructural examination and predictions of thermodynamic calculations.

2. Experimental procedure

2.1. Cycling scheme

Two stacks of four ML3X Zebra cells received from Fiamm SoNick were subjected to continuous charge–discharge cycles to the point of failure or a level of exaggerated cell resistance. The specifications of these cells are summarized in Table 1. One stack was cycled at the lower temperature limit, i.e., 260 °C, and the other at the upper temperature limit, 350 °C. Cells were vertically positioned in a specially designed oven provided by Fiamm SoNick. The cycling was performed using a Digatron UBT 6-50 battery testing unit. In order to accelerate damage, a more stressful charging regime was implemented (Fig. 1). The charging voltage limit was increased to the voltage of the overcharge

* Corresponding author. Tel.: +1 905 525 9140x27242.
E-mail addresses: hosseinifar.m@gmail.com (M. Hosseinifar), petric@mcmaster.ca (A. Petric).

0378-7753/$ – see front matter © 2012 Elsevier B.V. All rights reserved.
doi:10.1016/j.jpowsour.2012.01.125

Table 1
Characteristics of ML3X Zebra cells.

Nominal capacity (Ah)	Specific power ($W\,kg^{-1}$)	Power density ($W\,l^{-1}$)	Specific energy ($W\,h\,kg^{-1}$)	Weight (kg)	Dimension (cm)
38	245	280	140	0.685	$3.5 \times 3.5 \times 23$

reaction (3.1 V per cell). It is worth mentioning that in the Zebra batteries the cells rarely reach such a high voltage. Therefore, this charging profile represents an accelerated life test. The voltage limit increase allowed the current to remain at 10 A for 3 h, thus utilizing 30 Ah of capacity. The discharge consisted of a constant 15 A current applied for 2 h or to the point that the cell potential dropped below 1.72 V per cell. In contrast to charging, the current was abruptly shut off as soon as the voltage limit was reached. Temperature, applied current and cell voltages were recorded and used to monitor performance of the cells during the test.

2.2. Characterization methods

Degraded cells at the end of cycling were destructively opened in an argon atmosphere glove box. The cells were opened following one individual standard IU charging procedure. Both the positive electrode and the inner surface of the β″ alumina in contact with cathode were examined using scanning electron microscopy (SEM). The β″ pieces were soaked in acetone and cleaned in an ultrasonic bath for 1 min. Characterization of the positive electrode was done by SEM observation of fracture surfaces with no exposure to moisture or any other treatment. The constituent phases were identified by energy dispersive spectroscopy (EDS) and X-ray diffraction (XRD). The positive electrode of the ML3X Zebra cell is approximately 20 cm high. In order to thoroughly examine the microstructural changes, three samples taken at 2, 7 and 14 cm from the bottom of the cell were investigated.

Pieces of the positive electrode were washed with distilled water, thereby removing the salts – NaCl, $NiCl_2$ and $NaAlCl_4$. The remaining powder consisted almost exclusively of Ni particles. The size distribution of these particles was analyzed utilizing the liquid phase sedimentation technique. A homogeneous suspension of the powders in glycerol was achieved at room temperature using mechanical and ultrasonic stirring. The measurements were carried out with a Horiba CAPA700 particle size analyzer. The morphology of the Ni particles was examined with SEM and the phases were identified by XRD.

3. Results

3.1. Charge–discharge data

Fig. 2 shows the internal resistance of the cells at the end of charge for 260 °C and 350 °C tests. The resistance is estimated using the recorded current (I) and cell voltages (V) according to the following relationship:

$$R = \frac{E - V}{I} \quad (1)$$

where E is the open circuit voltage of the cell and is equal to 2.59 V at 260 °C and 2.57 V at 350 °C.

The impact of temperature on Zebra cell performance can be deduced by comparing Fig. 2a and b. In the low temperature test, the cells maintained low internal resistance for 300 cycles. At that point, a sudden increase in resistance occurred in 3 cells followed by progressive capacity loss over the next 3 cycles. The increase in resistance was accompanied by drift into the overcharge state. This led to complete failure in discharge as cell voltages dropped below the prescribed 1.72 V immediately upon switching into discharge mode. At 350 °C, the cells maintained relatively low resistances for 300 cycles similar to the low temperature test. Thereafter, they continued to work despite reaching much higher resistances where the overcharge voltage was far surpassed in 2 of the 4 cells (cell 1 reached 3.58 V at the end of cycling). There was gradual capacity loss throughout the test. The high temperature cells did not fail by drifting beyond the operating parameters as low temperature cells did. The test was stopped after 600 cycles for safety reasons.

Fig. 3 shows a comparison between c/4 (i.e., 9.5 A current) discharge rate of a new cell versus cells at the end of cycling. The cycled cells were removed from the stack and discharged separately at their respective temperatures. The new cell was discharged at 300 °C. The most striking feature of this graph is the significant decrease in the voltage of the cell cycled at 260 °C which translates

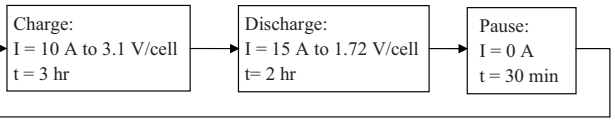

Fig. 1. Cycling scheme utilized in the present investigation.

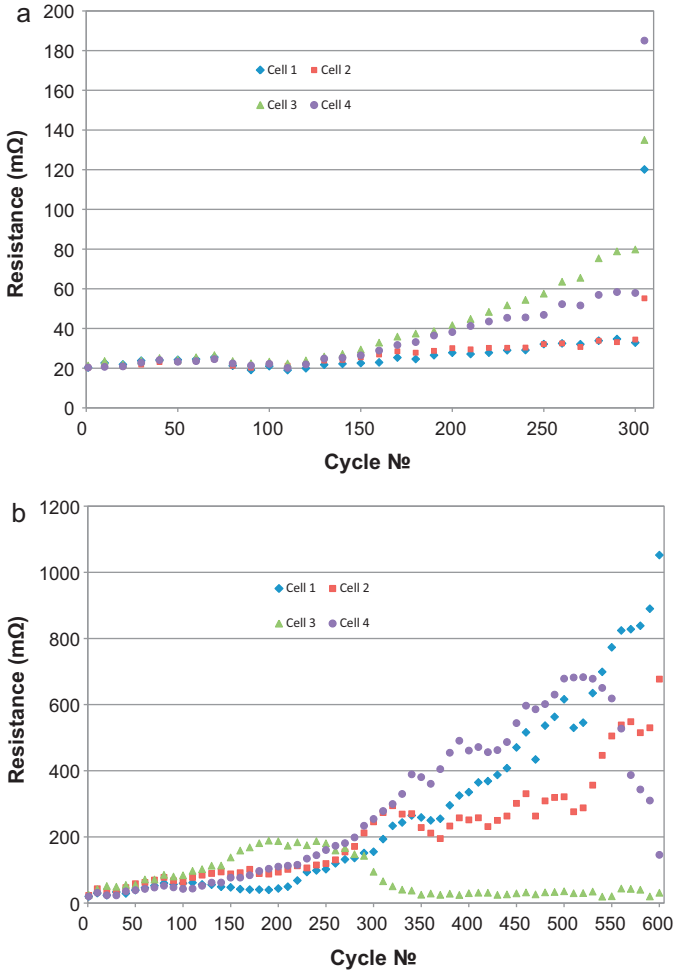

Fig. 2. The resistance at the end of charge for the cells cycled at (a) 260 °C and (b) 350 °C.

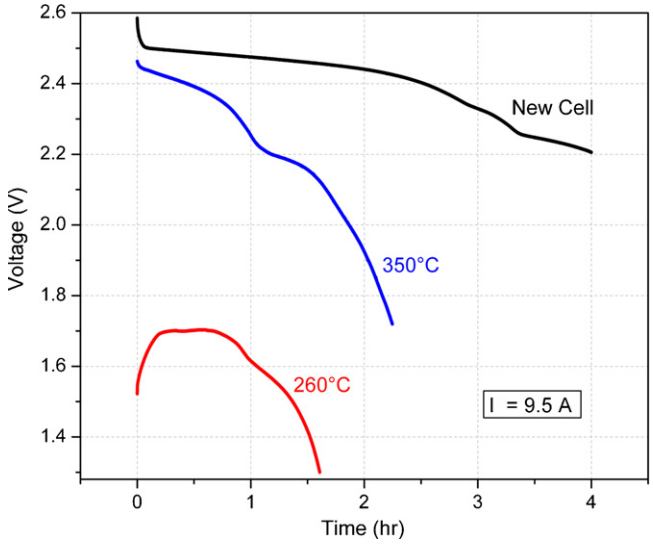

Fig. 3. Discharge behavior of single cells at the end of testing compared with that of a new cell.

into very high resistance build up in this cell. The voltage drop is more pronounced at the beginning of the discharge. Since the discharge reaction of the Zebra cell starts at the β″ electrolyte and moves toward the current collector, this pronounced drop indicates that the resistance build up has occurred adjacent to the solid electrolyte. As the discharge progresses, the reaction front moves away from the β″ interface and the voltage recovers to some extent. The discharge of this cell was arbitrarily stopped at 1.3 V. This phenomenon was not observed in cells cycled at 350 °C. However, a decrease in capacity of this cell is apparent since the cell is fully discharged after 2.5 h.

The same cells shown in Fig. 3 were charged individually with standard IU regime in order to measure their capacity. Fig. 4 shows that the cell cycled at 350 °C was unable to accept 10 A current for as long as a new cell. It had lost 38% of its capacity. A less severe capacity loss is observed in the cell cycled at 260 °C; however, it is even more noteworthy that this cell is unable to accept the nominal 10 A current at all. The immediate current drop supports the idea that a high resistance product is formed close to the β″ interface. The charge reaction also starts at β″ and because of this resistance build

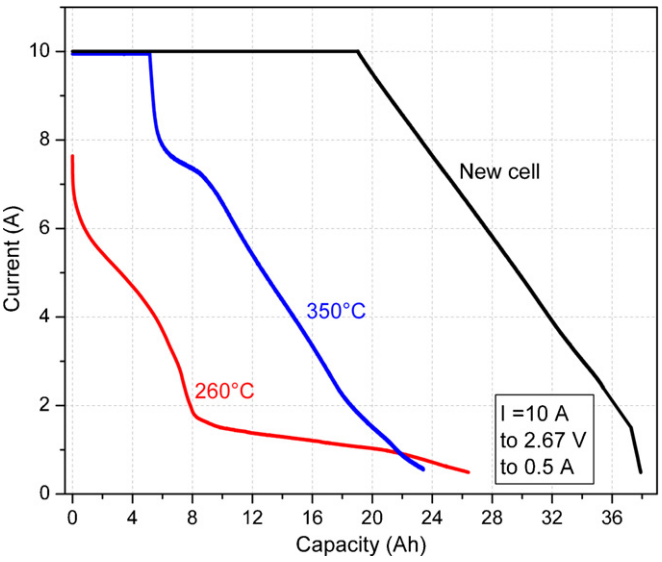

Fig. 4. Capacity and performance of individual cells under standard IU charging.

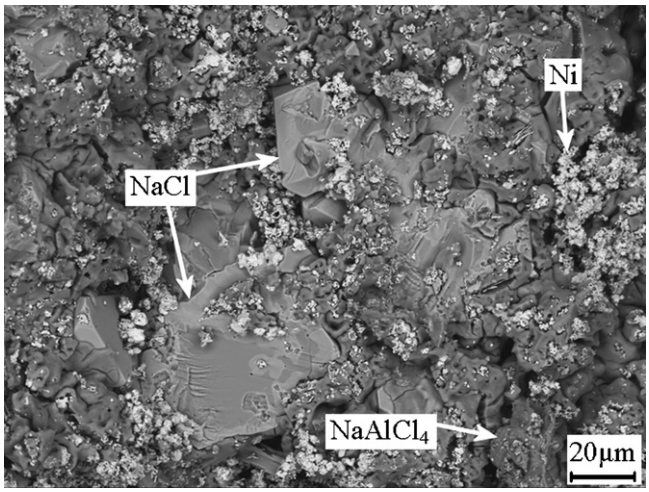

Fig. 5. SEM image of positive electrode from low temperature cell showing discharge products.

up, the limiting voltage of 2.67 V is reached as soon as the current is applied and charging is switched to voltage mode at decreased current. The cycled cells whose behavior is shown in Figs. 3 and 4 were opened in the fully charged state (at the end of IU charging). The cathode and the solid electrolyte were examined to identify the failure mechanism of low temperature cells and the cause of capacity loss in cells cycled at 350 °C.

3.2. Microstructural investigation

Beginning with the cell cycled at 260 °C, it was found that although the cell was supposedly fully charged, the positive electrode was only partially charged. NaCl particles of 60 μm length were observed in the core of the cathode 4 mm away from the solid electrolyte (Fig. 5). The growth of Ni particles can readily cause cell degradation in Zebra cells [11]. The small size (<2 μm) of Ni particles seen in Fig. 5 dismisses this as the cause of degradation in the low temperature cell. As expected, $NiCl_2$ was abundantly found in the charged portion of the cathode; surprisingly however, AlF_3 particles were observed in the positive electrode in contact with β″ (Fig. 6). This material is not an ingredient of the positive electrode but is formed during cycling.

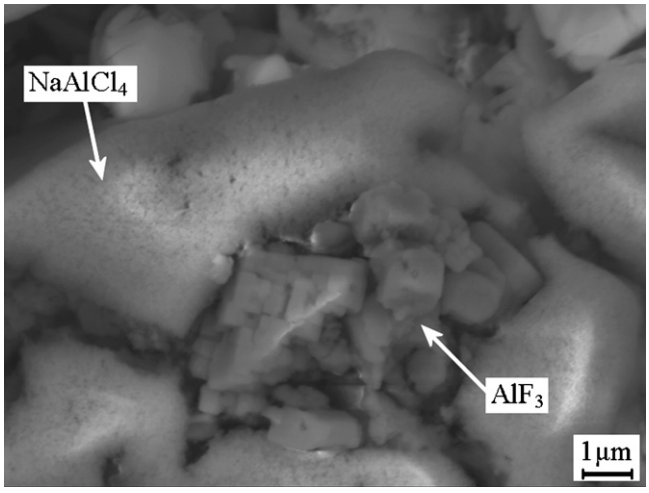

Fig. 6. AlF_3 particles in positive electrode adjacent to β″ ceramic in the cell cycled at 260 °C.

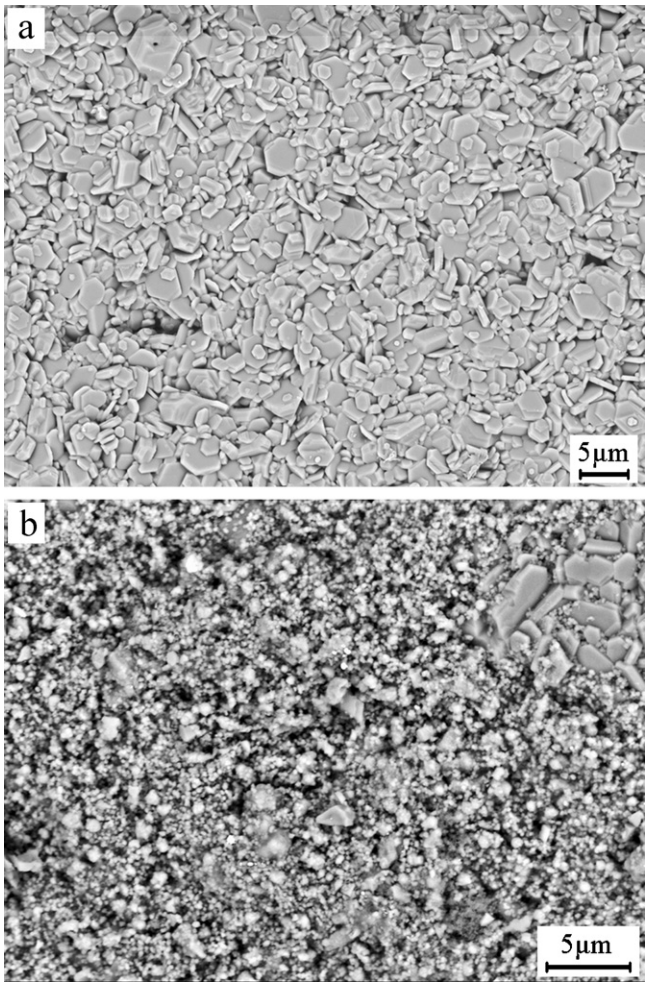

Fig. 7. The inside surface of solid electrolyte from (a) a new cell where only β″-alumina grains are seen and (b) a cell cycled at 260 °C showing widespread coverage by AlF_3.

AlF_3 particles were found to be widely dispersed on the inside surface of the ceramic electrolyte in contact with the cathode. Fig. 7a and b compares the surface of β″ from the new cell with that of the cell cycled at low temperature. The β″ grains are barely seen in Fig. 7b. Of course not the entire surface of the solid electrolyte was covered with these particles but the density of AlF_3 coverage was high enough to conclude that the formation of these particles is the cause of the resistance increase and subsequent failure of the cells cycled at 260 °C. It impedes the flow of sodium ions through β″ into and out of the cathode compartment.

Such widespread deposition of AlF_3 particles was not seen in the cells cycled at 350 °C. Only a few sizable AlF_3 particles were found (Fig. 8). The substantial resistance increase observed in the high temperature cells cannot be associated with these large and coarsely distributed particles. It is worth mentioning that no sign of Fe ion exchange with sodium was found in β″ alumina of either low or high temperature cells.

Disparities were observed in the state of charge of the cathode (nominally charged) for the cells cycled at 350 °C. While the lower half of the cell was fully charged, the upper half remained largely in the discharged state. Only a 1–2 mm layer of the cathode close to the β″ interface was charged in the upper part of the cell. Fig. 9 shows the microstructure of a sample taken at 14 cm from the bottom of the cell. Similar to Fig. 5 the discharge products (Ni and NaCl) are seen in this image, but unlike the low temperature cell, a significant

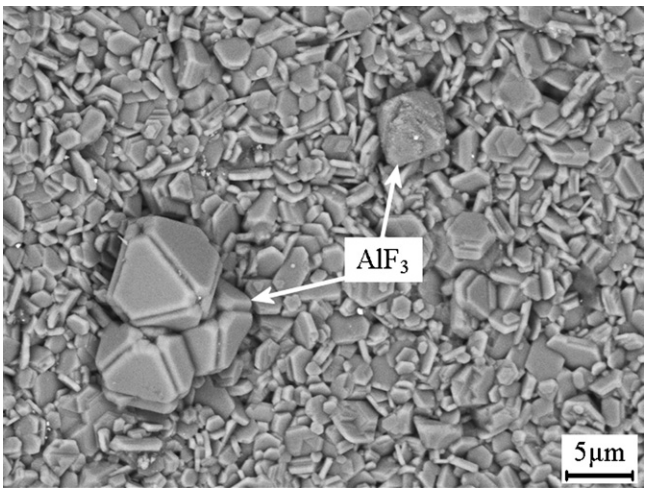

Fig. 8. Coarse AlF_3 particles formed on β″ surface at 350 °C.

increase in the size of Ni grains is observed. The average size of the original Ni powder is 2 μm.

The size distribution of the Ni particles of cycled cells is compared with that of the new cell in Fig. 10. More than 90% of Ni particles in the new cell and the low temperature cell are less than 10 μm in size. In fact some refinement of Ni particle size is observed due to cycling at 260 °C. On the other hand, a 30% decrease in the fraction of particles less than 10 μm in size is seen in the cells cycled at high temperature. The decrease is compensated by the formation of larger Ni grains up to 70 μm. This Ni grain growth is deemed to be the cause of capacity loss in the cells cycled at 350 °C.

There was a possibility that the large Ni particles were merely agglomerates of small grains. An SEM analysis of the extracted powder from the high temperature cell refuted this possibility. Fig. 11a and b shows the extracted powders from the as received cell and the cell cycled at 350 °C, respectively. An agglomeration of small particles (1–2 μm) is apparent in the as received cell. In contrast, individual particles grown larger than 10 μm can be easily recognized in the high temperature cell. A distinct ledge morphology is notable on the surface of the enlarged grains.

Another feature seen in Fig. 11b is particles of the Ni_3S_2 compound attached to the enlarged Ni grain. The formation of this compound was reported in earlier attempts to optimize the composition of the cathode in cases where the cell was cycled at high rates [11]. An XRD analysis of the extracted powders revealed that

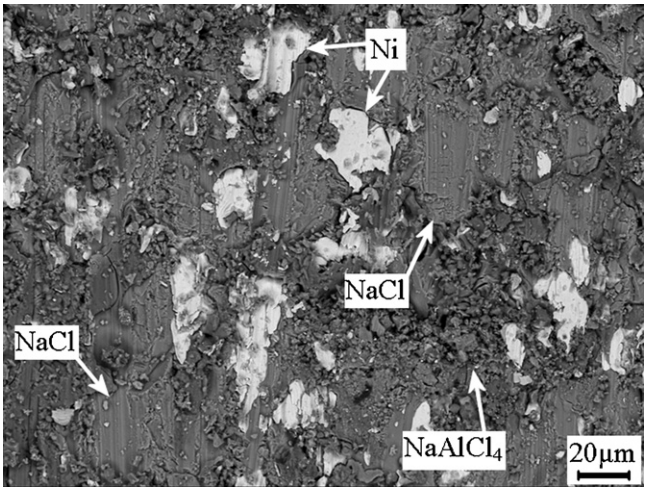

Fig. 9. Evidence of Ni particle growth in the cathode of a cell cycled at 350 °C.

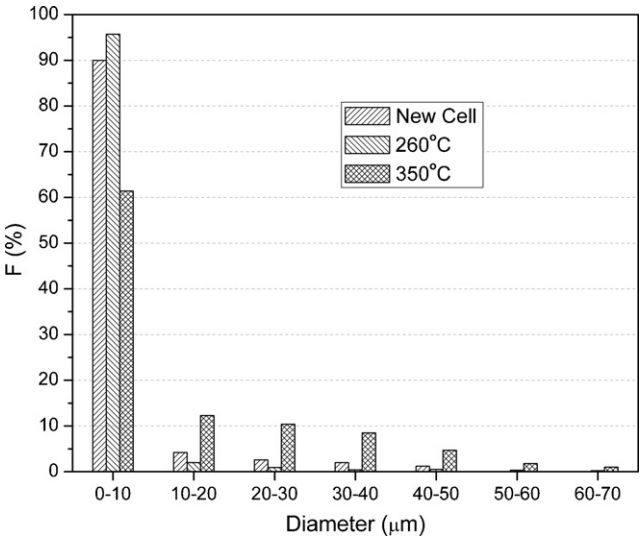

Fig. 10. Ni particle size distribution of cycled cells compared with that of the new cell.

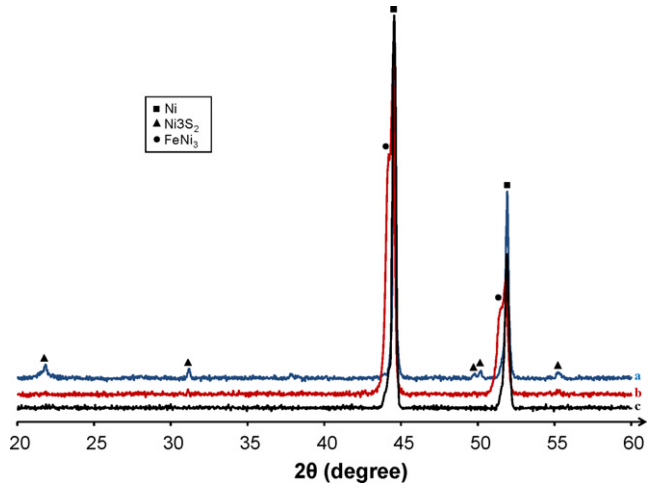

Fig. 12. XRD pattern of Ni powders extracted from cycled cells at (a) 350 °C, (b) 260 °C and (c) the new cell.

this phase did not exist in cells prior to cycling (Fig. 12). Traces of Ni_3S_2 were found in the cell cycled at 260 °C. However, it is the high temperature cell in which a noticeable increase in the amount of this phase was observed.

The Ni grain growth was less pronounced in the bottom half of the cell which is consistent with the fully charged state of this part. Fig. 13 shows an SEM image of the positive electrode taken 2 cm from the bottom of the cell. A rather dense layer is observed around the cathode in contact with β″-alumina electrolyte (the left hand side of the image). The constituent phases of this layer were identified as $NiCl_2$, Na_6FeCl_8 and Ni_3S_2 using XRD analysis (Fig. 14). The Na_6FeCl_8 compound is a transient phase formed in Na/$FeCl_2$ cells [12–14]. The formation of this phase is also found in a charged Zebra cell after only three cycles [15]. EDS examination of the $NiCl_2$ compound in this layer revealed that more than half of the Ni was substituted with Fe which resulted in a small shift in the position of $NiCl_2$ in XRD pattern. The formation of this layer may have played a role in the resistance increase of the cell as virtually no pure Ni or liquid electrolyte is detected in this layer.

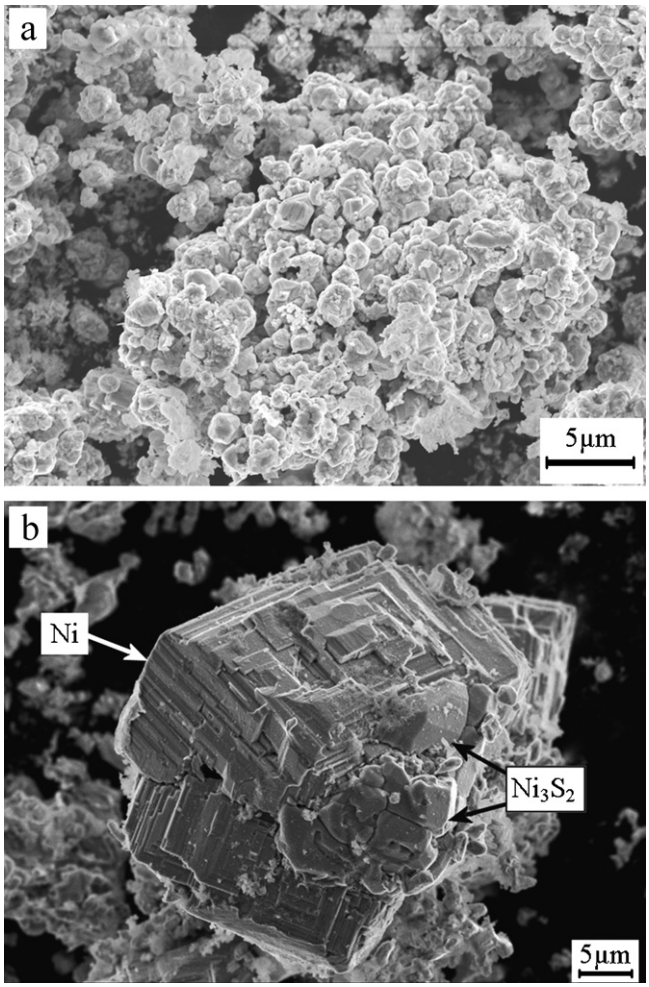

Fig. 11. SEM micrograph of Ni particles extracted from (a) a new cell and (b) a cell cycled at 350 °C.

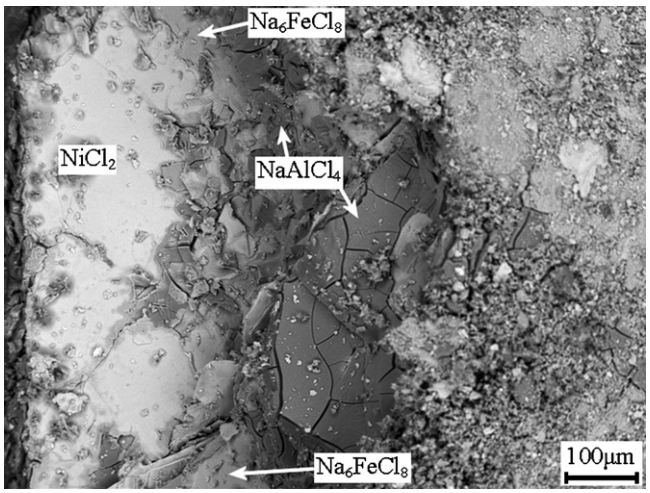

Fig. 13. Constituent phases of a layer formed on the surface of the positive electrode in contact with solid electrolyte 2 cm from the bottom of the cell cycled at 350 °C.

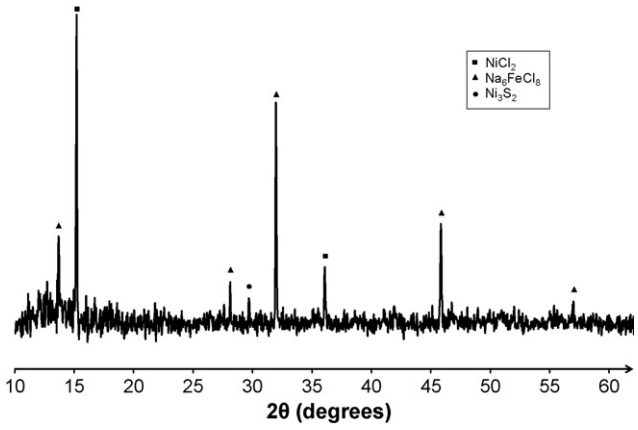

Fig. 14. XRD pattern of the surface layer shown in Fig. 13.

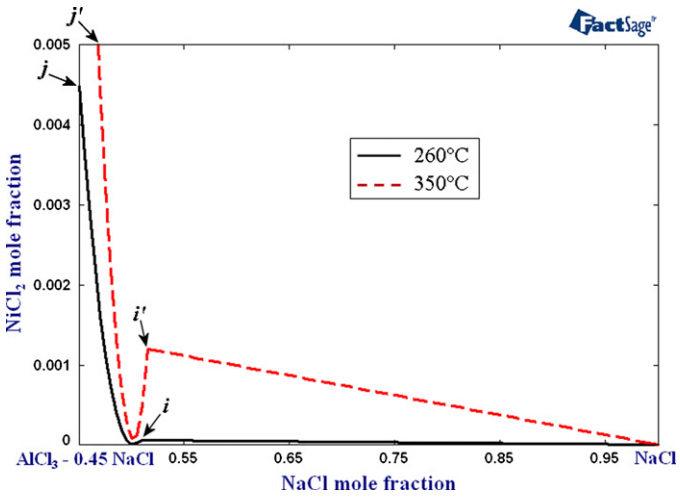

Fig. 15. The limits of $NiCl_2$ solubility in liquid electrolyte.

4. Discussion

Based on the results of cycling, it was established that the formation of a high resistance layer of AlF_3 on the surface of β″ led to the failure of the cells cycled at 260 °C. One may consider the source of fluorine and how AlF_3 is formed. Fluorine is added in the form of NaF. It was found that the addition of this compound and other sodium halides (NaI and NaBr) is beneficial in suppressing the $FeCl_2$ dissolution and provides a degree of overcharge protection [6]. Moreover, Prakash et al. [16,17] reported an improvement in the cell's impedance with the addition of NaI and NaBr. It is likely that at the operating temperature, NaF forms complex ions with the liquid electrolyte in the form of $Al(Cl_xF_{1-x})_4^-$ [18]. The presence of AlF_3 is not observed in cells cycled with the recommended IU charging profile. This observation suggests that the formation of AlF_3 is related to the overcharge condition due to the high charging voltage used for the accelerated life test. Let us consider the overcharge reaction of Zebra cells:

$$2NaAlCl_4 + Ni \rightarrow 2Na + NiCl_2 + 2AlCl_3$$

If it is supposed that the complex ions are formed within the chloroaluminate melt, the above reaction is revised as follows:

$$2NaAl(Cl_xF_{1-x})_4 + Ni \rightarrow 2Na + NiCl_2 + 2Al(Cl_yF_{1-y})_3$$

Since some of the chlorine in the liquid electrolyte is utilized in the formation of $NiCl_2$, the fluorine content of the $Al(Cl_yF_{1-y})_3$ product is increased. The AlF_3 may precipitate from this high fluorine containing compound. Similar to the normal cell reactions, the overcharge reaction also starts near β″ and moves inward. This explains the formation of AlF_3 on the ceramic electrolyte.

Although the same reaction is operative at higher temperatures, it is not clear why high temperature cells did not fail in a similar manner. A possible explanation may be that the lower viscosity of the liquid electrolyte at higher temperature allows it to compensate for the loss of chlorine before AlF_3 is formed. Moreover, the higher diffusivity of ions at high temperature can be instrumental in preventing the widespread formation of AlF_3.

Another mechanism for AlF_3 formation can be proposed by incorporating NaF into the overcharge reaction:

$$NaAlCl_4 + 3NaF + 2Ni \rightarrow 4Na + 2NiCl_2 + AlF_3$$

A thermodynamic calculation using FactSage [19] and the Fact53 database showed that the voltage of this reaction was too low (1.876 V at 260 °C and 1.86 V at 350 °C) to be considered functional.

Regardless of how AlF_3 is formed, it is crucial to understand that because of its high stability, upon formation, it cannot be removed by further treatments. All other aluminum halides are in the liquid state at cell operating temperatures while the melting point of AlF_3 is 1291 °C. If NaI and NaBr provide the benefits associated with NaF, then the formation of AlF_3 can be avoided by simply not adding the NaF in the first place. It is possible that the low temperature cells would have worked longer at low resistance had AlF_3 not formed.

At 350 °C, nickel grain growth seems to be the most probable cause for capacity loss. A Ni backbone that is formed by interconnected fine nickel particles provides electronic conductivity from current collector to β″. The growth of Ni grains interrupts this connection and makes it difficult for electrons to reach the reaction front. It also decreases the surface area for reaction.

The enabling effect of high temperatures on grain size increase is well known in metals and alloys and can readily be the cause of Ni particle growth in the high temperature test; nevertheless, contributions from other factors need to be included. Fig. 15 illustrates the solubility of $NiCl_2$ in the liquid electrolyte at the two cycling temperatures used in the present investigation. These calculations are performed using FactSage and the FTsalt database. During charging, the NaCl is consumed and the cathode composition moves left in this diagram. Points *i* and *i*′ represent the maximum solubility of $NiCl_2$ for the normal cell operation at 260 °C and 350 °C, respectively. It can be seen from this diagram that the solubility of $NiCl_2$ is much higher at 350 °C than at 260 °C (0.16 wt% versus 0.0076 wt%). If the cell is overcharged, the solubility of $NiCl_2$ varies according to the curved *ij* and *i*′*j*′ lines for 260 °C and 350 °C, respectively. It is interesting to note that $NiCl_2$ dissolution actually decreases with slight overcharging of the cell before rising drastically at deeper overcharge. The low temperature cells were briefly and slightly overcharged before failure. On the other hand, three of the high temperature cells experienced many cycles in which deep overcharge occurred. An excessive $NiCl_2$ dissolution and subsequent Ni grain growth is expected to have occurred in these cells.

Another factor that may have contributed to the growth of Ni particles is the formation of the Ni_3S_2 compound. Sulfur is key in preventing the grain growth by poisoning the surface of nickel particles [11]. The formation of Ni_3S_2 consumes sulfur and reduces the capacity of this mechanism. It can be speculated that higher initial sulfur content would offset Ni_3S_2 formation and prevent capacity loss. Verifying such speculation requires a more fundamental understanding of how Ni_3S_2 forms and what are the controlling factors. For example, it is not clear whether Ni_3S_2 is formed due to faster kinetics at high temperatures or merely cycling. This phase is also formed, although in smaller amounts, in the cells tested at 260 °C. Considering the fact that the high temperature cells underwent twice as many charge–discharge cycles, cycling may be the

controlling factor. Nevertheless, it must be realized that high sulfur content has adverse effects on normal cell operation [20] and an optimum amount is empirically found and added to the commercial cell.

5. Conclusions

Zebra cells were cycled at the extremes of temperature range employing an aggravated charge–discharge regime. The degradation of the cells was related to microstructural changes characterized by SEM and XRD analysis of positive electrode and solid electrolyte. The following results were obtained:

(1) The cells cycled with a charging voltage of 3.1 V per cell underwent a noticeable degradation both at 260 °C and 350 °C. Compared to the recommended charging profile, the accelerated one is responsible for the onset of overcharge reactions that induce a large resistance increase. In spite of that, the cells were able to operate for hundreds of cycles.
(2) The cells cycled at 260 °C maintained low resistance for 300 cycles before rapid failure occurred in discharge mode. The failure occurred following a few cycles in which cells were slightly overcharged.
(3) The charge and discharge behavior of the low temperature cells indicated that a high resistance layer formed close to the solid electrolyte. This layer was identified as AlF_3 particles deposited on the surface of β″ alumina. It is speculated that this phase precipitates from the fluorine enriched overcharge product $Al(Cl_yF_{1-y})_3$.
(4) The cells cycled at 350 °C did not fail in the manner observed in low temperature cells. AlF_3 was only seen in the form of coarse particles. Nonetheless, by the end of cycling, these cells showed high internal resistance, severe capacity loss and underwent deep overcharges.
(5) The growth of Ni particles is attributed the cause of capacity loss in the cells cycled at 350 °C. A combination of high temperature, increased $NiCl_2$ dissolution in molten electrolyte and the formation of Ni_3S_2 phase are believed to be responsible for Ni grain growth in high temperature cells.

Acknowledgements

We wish to thank Dr. Alberto Turconi at Fiamm SoNick for providing the Zebra cells and we acknowledge the financial support from NSERC and Vale Canada Inc.

References

[1] X. Lu, G. Coffey, K. Meinhardt, V. Sprenkle, Z. Yang, J.P. Lemmon, Electochem. Soc. Trans. 28 (2010) 7–13.
[2] X. Lu, J.P. Lemmon, V. Sprenkle, Z. Yang, JOM 62 (2010) 31–36.
[3] J. Coetzer, J. Power Sources 18 (1986) 377–380.
[4] A. van Zyl, Solid State Ionics 86–88 (1996) 883–889.
[5] H. Bohm, G. Beyermann, J. Power Sources 84 (1999) 270–274.
[6] R.C. Galloway, S. Haslam, J. Power Sources 80 (1999) 164–170.
[7] J.L. Sudworth, J. Power Sources 100 (2001) 149–163.
[8] C.H. Dustmann, J. Power Sources 127 (2004) 85–92.
[9] R. Tilly, R.C. Galloway, Electric Vehicle Symposium 18, Berlin, 2001.
[10] P.T. Moseley, R.J. Bones, D.A. Teagle, B.A. Bellamy, W.M. Hawes, J. Electrochem. Soc. 136 (1989) 1361–1368.
[11] R.J. Bones, D.A. Teagle, S.D. Brooker, F.L. Cullen, J. Electrochem. Soc. 136 (1989) 1274–1277.
[12] K.T. Adendorff, M.M. Thackeray, J. Electrochem. Soc. 135 (1988) 2121–2123.
[13] N.D. Nicholson, D.S. Demott, R. Hutchings, Proceedings of the 16th International Power Sources Symposium Committee, Bournemouth, UK, 1988, p. 549.
[14] J. Coetzer, G.D. Wald, S.W. Orchard, J. Appl. Electrochem. 23 (1993) 790–800.
[15] T. Javadi, A. Petric, J. Electrochem. Soc. 158 (2011) A700–A704.
[16] J. Prakash, L. Redey, D.R. Vissers, J.D. Ggruson, J. Appl. Electrochem. 30 (2000) 1229–1233.
[17] J. Prakash, L. Redey, D.R. Vissers, Ionics 6 (2000) 210–217.
[18] B. Gilbert, S.D. Williams, G. Mamantov, Inorg. Chem. 27 (1988) 2359–2363.
[19] http://www.factsage.com/ (accessed 01.11.11).
[20] B.V. Ratnakumar, S. Surampudi, G. Halpert, J. Power Sources 48 (1994) 349–360.